




Mechanosensitive bonds induced complex cell motility patternsJen-Yu Lo ¹, Yuan-Heng Tseng,¹ and Hsuan-Yi Chen ^{1,2,3,*}¹*Department of Physics, National Central University, Zhongli 32001, Taiwan*²*Institute of Physics, Academia Sinica, Taipei 11529, Taiwan*³*Physics Division, National Center for Theoretical Sciences, Taipei 10617, Taiwan* (Received 10 January 2023; revised 19 September 2023; accepted 19 January 2024; published 13 February 2024)

The one-dimensional crawling movement of a cell is considered in this theoretical study. Our active gel model shows that a moving cell with weakly mechanosensitive adhesion complexes tends to move at constant velocity. As the mechanosensitivity of the adhesion complexes increases, a cell with sufficiently strong myosin contractile or high actin polymerization rate can exhibit stick-slip motion. Finally, a cell with highly mechanosensitive adhesion complexes exhibits periodic back-and-forth migration. A simplified model that assumes that the cell crawling dynamics are controlled by the evolution of the myosin density dipole and the asymmetry of adhesion complex distribution captures the motility behaviors of crawling cells qualitatively. It suggests that complex cell crawling behaviors could result from the interplay between the distribution of contractile force and mechanosensitive bonds.

DOI: [10.1103/PhysRevResearch.6.013164](https://doi.org/10.1103/PhysRevResearch.6.013164)**I. INTRODUCTION**

The crawling motion of eukaryotic cells is ubiquitous in biology as it plays important roles in processes such as embryogenesis, wound healing, cancer metastasis, and immunology [1]. Common if not universal features of a crawling cell include myosin motors distributed mainly behind the center, dominant actin polymerization in the leading edge, and higher density of adhesion complexes in the leading region [2]. Such polarized molecular distribution enables protrusion in the leading edge due to actin polymerization, treadmilling of the actomyosin cytoskeleton due to contractility, and traction force pulling the cell body. These features are included in many theoretical models for crawling cells [3].

Besides nonmotile resting and steady-moving behaviors, cells crawling along a one-dimensional track either on a substrate or in a three-dimensional environment also exhibit moving patterns that are nonstationary in time. For example, stick-slip crawling motion due to slip between integrin and the extracellular matrix in focal adhesions under the contractility provided by myosin II has been observed in human osteosarcoma cells [4]. Periodic back-and-forth migration has been observed in crawling zyxin-depleted cells in a collagen matrix [5] and dendritic cells crawling along microfabricated channels [6].

Several theoretical models were proposed to explain some deterministic complex moving patterns. A model with the

mechanochemical couplings of actin promotor, actin polymerization, and myosin kinetics was shown to produce periodic back-and-forth migration [7]. On the other hand, a mechanical model emphasizing the interplay between the mechanosensitive bonds and membrane tension exhibited stick-slip motion even for slip bonds [8]. Interestingly, it has also been shown that stick-slip can result from the interplay between mechanosensitive bonds, contractility, and a force that restores a cell's preferred length [9].

From the aforementioned experimental and theoretical studies, it is natural to ask whether all of the one-dimensional deterministic complex cell moving patterns can be found in one theoretical model that contains only the essential mechanical components related to cell crawling. Since some of the complex cell moving patterns, for example, back-and-forth migration, involve changes in the cell polarity, an important goal of this model is to generate such cell polarity changes autonomously. Furthermore, because the relevant length and time scales of the problems under consideration are much longer than those in the molecular scale, a hydrodynamic model with only a few slow variables is preferred, and the goal is to understand what cooperative effects help to generate those complex cell moving patterns.

In this article, we present a theoretical study to show that the coupling between mechanosensitive adhesion complexes and myosin contractility is sufficient to generate deterministic complex cell crawling behaviors, including stick-slip, periodic back-and-forth, and other complex moving patterns. Since our approach is hydrodynamical, molecular details are not important in the two models presented in this article. The most essential ingredients are adhesion complexes that appear close to the cell ends, active contractile cytoplasm that contains myosin motors, and actin polymerization at cell ends. The two models we construct reproduce the following key properties related to these components. For a cell at rest, the

*hschen@phy.ncu.edu.tw

Published by the American Physical Society under the terms of the [Creative Commons Attribution 4.0 International license](https://creativecommons.org/licenses/by/4.0/). Further distribution of this work must maintain attribution to the author(s) and the published article's title, journal citation, and DOI.

adhesion complexes aggregating close to the cell ends, the myosin motors aggregating close to the center of the cell, and actin polymerization at cell ends are all symmetric. When a cell moves, this symmetry is broken as adhesion complexes aggregate close to the leading cell end, myosin motors aggregate close to the trailing end, and actin polymerization in the leading edge dominates.

In the first model, which we call the active gel model, the association and dissociation of the adhesion complexes are allowed to take place anywhere in the cell, and the corresponding rates are chosen to be of the simplest forms that make the spatial distribution of adhesion complexes agree qualitatively with experimental observations. In the second model, which we call the simplified model, the adhesion complexes are allowed to appear close to the cell ends only, and the evolution of the number of adhesion complexes is more general than what we chose in the active gel model. In both models, we find that the distributions of adhesion complexes and myosin motors and the polarization of actin polymerization agree qualitatively with experimental observations. Furthermore, complex cell crawling behaviors are found, and the mechanism for autonomous cell polarity reversal is clarified. Our results show that, as long as myosin motors are pulled toward the cell end with more adhesion complexes as a result of contractility, and the number of adhesion complexes near the cell end that is more distant from the peak position of myosin density increases sufficiently rapidly due to mechanosensitivity, motility behaviors that are periodic in time can be found.

This article is organized in the following way. In Sec. II, we present our active gel model with mechanosensitive adhesion complexes. We show that by varying myosin contractility, actin polymerization rate, and mechanosensitivity of the adhesion complexes, this model can exhibit complex motility behaviors other than rest and constant-velocity moving states. A moving cell with weakly mechanosensitive adhesion complexes exhibits constant velocity motion, while a cell with highly mechanosensitive adhesion complexes exhibits periodic back-and-forth movement. Stick-slip and other complex motility patterns can be observed by increasing the mechanosensitivity of the adhesion complexes for a moving cell with high contractility or actin polymerization rate.

To understand the physical mechanisms that produce these complex motility patterns, a simplified model is constructed in Sec. III. This model shows that, in general, the dynamics of a slow-moving cell can be determined by the dipole moment of myosin density y_c , the total number of adhesion complexes N , and the difference in the number of adhesion complexes near the two cell ends ΔN . It shows that the coupled dynamics of these physical quantities can produce the complex motility behaviors found in our active gel model. The motility phase diagram of the simplified model is qualitatively similar to that of the active gel model. This suggests that the complex motility behaviors can result from the interplay of the dynamical organization of the mechanosensitive adhesions and the myosin motors.

In Sec. IV, we discuss the relation between our findings and existing experimental moving cell studies. Possible extensions of our model and future works are also discussed. Detailed discussions on modeling the mechanosensitivity of adhesion

complexes, the numerical methods and choices of parameters, and the construction of the simplified model are presented in Appendices.

II. ACTIVE GEL MODEL

In this model, the cytoplasm of the cell is treated as an active gel [10,11] enclosed by the cell membrane, the adhesion complexes are treated as reversible bonds with specific binding-unbinding rates, and actin polymerization is assumed to happen only at the cell ends. The forces acting on the cytoplasm include the stress in the gel, the drag force from the substrate, and the force due to the adhesion complexes.

Our model only considers the cell's moving direction. The stress in the cytoplasm obeys the constitutive equation $\sigma = \eta \partial v / \partial x + \chi c$, where η is the effective one-dimensional viscosity of the cytoplasm, v is the flow field of the gel, χ is the strength of contractility provided by myosin motors ($\chi > 0$), and c is the concentration of myosin attached to the actin network. For simplicity, compressibility is not included [11]. Thus, pressure does not appear in the constitutive relation. The cytoplasm also experiences drag forces from the substrate and the adhesion complexes. On the molecular scale, an adhesion complex sticking to the extracellular substrate is attached to actin bundles by specific proteins, and it experiences a contractile force of myosin through the actin bundles [12]. However, actin bundles do not appear explicitly in our active gel model, and the effect of myosin motors is described by contractile stress in the gel. Therefore, the intracellular force on the adhesion complexes at this level of description is modeled as an effective drag between the moving gel and the fixed adhesion complexes. This leads to a total drag force density that is the sum of the drag between the gel and the adhesion complexes, and the drag between the gel and the substrate, i.e., $F_{\text{drag}} = -\alpha n_b v - \xi v$. Here n_b is the density of the adhesion complexes, α is a constant that characterizes the drag from the adhesion complexes, and ξ is the drag coefficient from the drag of the substrate. Putting the force density due to the stress gradient and the force density from drag together, the resulting force balance equation is

$$\eta \frac{\partial^2 v}{\partial x^2} - (\alpha n_b + \xi) v = -\chi \frac{\partial c}{\partial x}. \quad (1)$$

Myosin motors attached to actin filaments move with the cytoplasm, while those detached from actin filaments diffuse freely. At timescales longer than that for myosin attachment/detachment, the density of the motors can be effectively described by an advection-diffusion equation [13]

$$\frac{\partial c}{\partial t} = D \frac{\partial^2 c}{\partial x^2} - \frac{\partial (cv)}{\partial x}, \quad (2)$$

where D is the effective diffusion coefficient of myosin motors. Note that c denotes the total local myosin density in our model. Therefore, the above equation contains the contribution from the free diffusing motors and the motion of myosin motors bound to the actin filaments. This also indicates that the coefficient χ is the contractile stress exerted by a motor averaged over timescales large compared to the myosin turnover time.

On the molecular scale, adhesion complexes are molecular aggregates composed of linkers (e.g., integrins) that provide anchorage to the extracellular matrix and other associated proteins [14]. Adhesion complexes are attached to actin bundles and pulled by the myosin motors on the actin bundles. It is known experimentally that an adhesion complex matures when a proper pulling force is applied, and dissociates when the pulling force vanishes [12]. In Appendix A, we present an analysis of the force dependence of the chemical potential of an adhesion complex from the thermodynamic point of view [12,14,15]. This analysis shows that the chemical potential of an adhesion complex depends on the total force (which is proportional to local gel flow v) and the tension (which is proportional to $\partial_x v$) acting on it. This means that if the association/dissociation of an adhesion complex is a passive process, the chemical potential of an adhesion complex should be a nonmonotonic function of v , and it should decrease as $\partial_x v$ increases. On the other hand, besides being mechanosensitive, the growth of adhesion complexes is also regulated by molecules not included in our active gel model [16]. Therefore a model including all these features will contain quite a lot of details. Another possible approach is to compose a minimal model inspired by the above information and validate such a minimal model by comparing the resulting spatial distribution of adhesion complexes with the experimental observations. This is the approach taken by our active gel model.

Since the chemical potential of an adhesion complex depends on v and $\partial_x v$, we assume that the dissociation rate of an adhesion complex is also a function of v and $\partial_x v$. In a previous study, we assumed that the association rate of an adhesion complex is a constant, and we modeled the dissociation rate as functions of v only [17]. The resulting distribution of adhesion complexes did not resemble the experimental observations. In this work, we assume the dissociation rate of an adhesion complex to be a decreasing function of $\partial_x v$, and the association rate to be a constant. We show that this model produces spatial distributions of adhesion complexes qualitatively agreeing with experimental observation. Since the effect of adhesion complexes on cell movement only appears in the $\alpha n_b v$ term of the force balance Eq. (1), our model is sufficient to study how mechanosensitive bonds affect the motility behaviors of a cell. In our model, once an adhesion complex is formed, it can be stretched by the cytoplasmic flow, but it does not flow with it [18]. Furthermore, we neglect the force dependence of the association rate but allow the stretching of cytoplasmic flow to increase the lifetime of an adhesion complex. The resulting evolution for n_b is

$$\frac{\partial n_b}{\partial t} = -k_0 e^{-k_1 \partial_x v} n_b + k_{\text{on}}, \quad (3)$$

where k_{on} is a constant. k_0 is the dissociation rate at $\partial_x v = 0$, and k_1 tells us how the dissociation rate is affected by the stretching effect of the cytoplasmic flow.

Besides being regulated by the force on the cell ends against actin polymerizations, actin polymerization at the cell ends also depends on the distribution of actin activators [19–22]. In the presence of environmental cues, a gradient of actin activator concentration within the cell is established, and actin polymerization is polarized due to this concentration gradient. In the absence of such external influence, the

cell can nevertheless polarize itself by spontaneous symmetry breaking. Once the cell starts to move, the actin activators are redistributed in the cell such that the net actin polymerization rate at the cell ends becomes asymmetric. In our model, we assume fast redistribution of actin activators in a moving cell such that the net actin polymerization velocity v_p^\pm at the \pm end of the cell is affected by the motion of the cell immediately. Furthermore, v_p^\pm also depends on the length of the cell because the cell has a restoring force to prevent it from collapsing under contractility or being stretched unlimitedly by actin polymerization [9,23,24]:

$$v_p^\pm = \frac{2 e^{-v_p^{(1)}(L-L_0)}}{1 + \exp\left[\mp \frac{dl_\pm}{dt} / v_p^{(2)}\right]} v_p^{(0)}, \quad (4)$$

where v_p^+ (v_p^-) is the net rate of extension due to actin polymerization at the cell end located at $x = l_+$ (l_-), and $L = l_+ - l_-$ is the length of the cell. $v_p^{(0)}$ represents the base polymerization velocity; $v_p^{(1)}$ comes from the effect of free energy cost for polymerization when the cell length is different from its natural length L_0 ; it slows down actin polymerization when L is large because of the force that tries to bring L back to L_0 (notice that the dimension of $v_p^{(1)}$ is inverse length). The term with $v_p^{(2)}$ makes the net polymerization rate in a moving cell higher in the leading end and lower in the trailing end.

The numerical solution of our model shows that both the mechanosensitivity of adhesion complexes and actin polymerization affect the possible complex cell motility patterns. Furthermore, the analysis in our simplified mode in Sec. III suggests that the main physical picture of our study is related to the symmetry properties of the dynamics of adhesion complexes and actin polymerization. Thus, the details of the association/dissociation rates of the adhesion complexes and the polymerization rate in our active gel model are unimportant.

The evolution of cell-end positions is determined by the velocity of the gel and actin polymerization,

$$\frac{dl_\pm}{dt} = v_\pm \pm v_p^\pm, \quad (5)$$

where v_+ (v_-) is the velocity of cytoplasm at the + (–) end.

Experimentally, it has been shown that a cell tends to restore its length L to L_0 [23]. We model this effect by the following force balance condition at cell ends:

$$\sigma_\pm = \left[\chi c + \eta \frac{\partial v}{\partial x} \right]_{l_\pm} = -\gamma(L - L_0). \quad (6)$$

Here, γ is a constant associated with the restoring force that brings the cell length L to L_0 .

Because no myosin motors can leave or enter the cell, the total flux of myosin motors across a cell end should vanish; i.e.,

$$[cv]_{l_\pm} - [c]_{l_\pm} \frac{dl_\pm}{dt} - D \left[\frac{\partial c}{\partial x} \right]_{l_\pm} = 0. \quad (7)$$

The first two terms are the advective flux relative to the moving cell end, and the third term is the diffusive flux at the cell end.

We introduce effective drag coefficient $\xi_{\text{eff}} = \xi + \alpha k_{\text{on}}/k_0$ and choose $l_0 = \sqrt{\eta/\xi_{\text{eff}}}$ as the unit length, $t_0 = \eta/(\xi_{\text{eff}} D)$ as

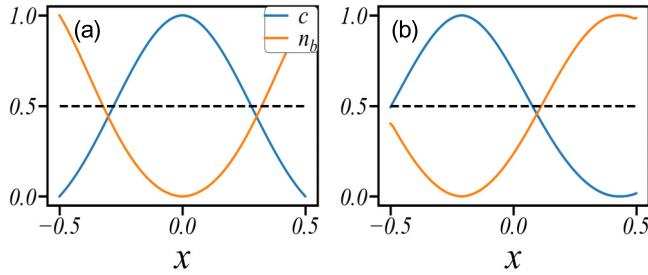


FIG. 1. Normalized densities of myosin motors and adhesion complexes for a cell (a) at rest and (b) undergoing constant velocity motion toward the $+x$ direction. The parameters are $K = 100$, $\tilde{\xi} = 1/3$, $k_{\text{on}} = 6$, $k_0 = 3$, $v_p^{(0)} = 0.2$, $v_p^{(1)} = 0.5$, and $v_p^{(2)} = 2$, and (a) $k_1 = 0.25$, $\tilde{\chi} = 16$, (b) $k_1 = 0.1$, $\tilde{\chi} = 16$.

the unit time, $\sigma_0 = \xi_{\text{eff}} D$ as the unit stress, $n_0 = \xi/\alpha$ as the unit density for adhesion complexes, and $c_0 = M/\sqrt{\eta/\xi_{\text{eff}}}$ as the unit myosin concentration, where M is the total number of myosin motors in the cell. Therefore the dimensionless drag coefficient $\tilde{\xi} = \xi/(\xi + \alpha k_{\text{on}}/k_0)$, contractility $\tilde{\chi} = c_0 \chi/\sigma_0$, and cell elastic constant $K = \gamma l_0/\sigma_0$ are used in the following discussion.

Numerical solutions of the active gel model. In general, our active gel model cannot be solved analytically. We numerically integrate the equations of motion by a finite-difference method. The details of our numerical methods and our choice of parameters are presented in Appendix B. For simplicity, we drop all the overbars of the dimensionless rate constants in the following. The numerical solutions show that, by varying the mechanosensitivity k_1 of the adhesion complexes, the strength of contractility, or the actin polymerization velocity, a cell can be at rest, moving with constant velocity, performing stick-slip, back-and-forth, or other periodic complex patterns.

Before discussing the motility behaviors of the cell, let us first check whether our active gel model produces qualitatively reasonable myosin and adhesion complex densities in rest and moving cells. Figure 1 shows that when the cell is at rest, myosin motor distribution is symmetric around the

center of the cell, and the number of adhesion complexes near both cell ends is the same; for a cell moving at constant velocity, myosin motors aggregate behind the center of the cell and adhesion complexes are mainly close to the leading end. Indeed, the evolution Eq. (3) of the adhesion complexes and the net actin polymerization at the cell ends Eq. (4) in our model leads to reasonable distributions for the key molecules in a cell. Notice that from the equations of motion and the boundary conditions, in the absence of actin polymerization, i.e., when $v_p^{(0)} = 0$, n_b and c are constants when the cell is at rest. This is also found in our numerical solutions (data not shown). Since such distributions of adhesion complexes and myosin motors do not resemble real cells, in this article we only consider cells with actin polymerization (i.e., $v_p^{(0)} \neq 0$).

Figure 2 shows the motility phase diagram for a cell with parameters chosen to be compatible with typical cells. The following motility behaviors are found: rest, constant velocity, unidirectional stick-slip movement, back-and-forth motion with stick-slip, and periodic back-and-forth movement. For a cell with weakly mechanosensitive adhesion complexes, as contractility increases, a cell at rest starts to move at constant velocity. As the adhesion complexes become more mechanosensitive, a moving cell shows other complex motility behaviors: for example, stick-slip motion and (at high contractility) back-and-forth motion with stick-slip. Finally, the cell performs periodic back-and-forth motion when the adhesion complexes are highly mechanosensitive.

The distributions of myosin motors and adhesion complexes for a cell that undergoes stick-slip and periodic back-and-forth movements are shown in Fig. 3. It is clear that even for these complex moving patterns, when the cell has a definite moving direction, myosin motors aggregate in a regime behind the center of the cell, and more adhesion complexes form near the leading end than the trailing end.

Figure 4 shows the phase diagram in the plane spanned by $v_p^{(0)}$ and k_1 . From this figure, we can see how the actin polymerization rate affects the motility behavior of the cell. The moving state of a cell with small k_1 is that with a constant velocity, while the moving state of a cell with large k_1 is

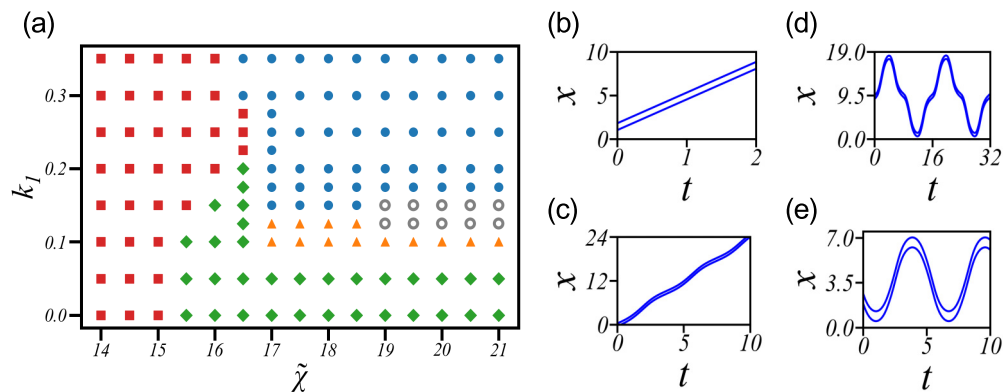


FIG. 2. (a) Motility phase diagram for a cell with $K = 100$, $\tilde{\xi} = 1/3$, $k_{\text{on}} = 6$, $k_0 = 3$, $v_p^{(0)} = 0.2$, $v_p^{(1)} = 0.5$, and $v_p^{(2)} = 2$. Rest state (squares), constant-velocity motion (diamonds), stick-slip movement (triangles), back-and-forth with stick-slip motion (empty circle), and periodic back-and-forth motion (filled circles) are found. (b) Trajectories of the cell ends for $\tilde{\chi} = 18$, $k_1 = 0.05$; the cell performs constant velocity motion. (c) Trajectories of the cell ends for $\tilde{\chi} = 17.5$, $k_1 = 0.1$; the cell performs stick-slip motion. (d) Trajectories of the cell ends for $\tilde{\chi} = 19$, $k_1 = 0.15$; the cell performs complex motility pattern which is periodic back-and-forth with stick-slip. (e) Trajectories of the cell ends for $\tilde{\chi} = 18$, $k_1 = 0.25$; the cell performs periodic back-and-forth motion.

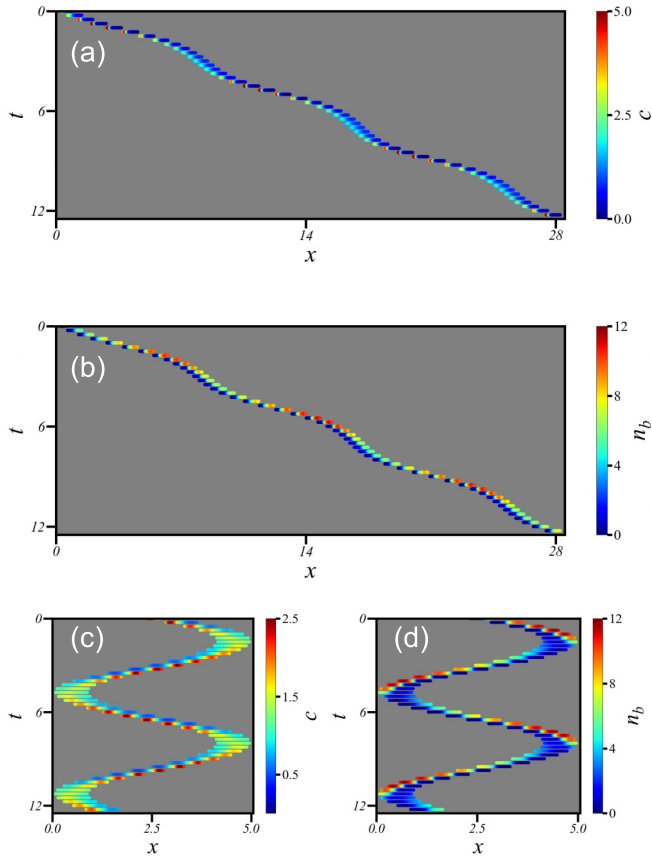


FIG. 3. Distribution of adhesion complexes and myosin motors for $K = 100$, $\xi = 1/3$, $k_{\text{on}} = 6$, $k_0 = 3$, $v_p^{(0)} = 0.2$, $v_p^{(1)} = 0.5$, $v_p^{(2)} = 2$, and (a), (b) $k_1 = 0.12$, $\bar{\chi} = 18$; (c), (d) $k_1 = 0.25$, $\bar{\chi} = 17$.

periodic back-and-forth. This agrees with the phase diagram in Fig. 2. Furthermore, there are several complex motility patterns between these two states, including stick-slip motion and behaviors that can be seen as combinations of back-and-forth and stick-slip movement. The trajectories for stick-slip movement and periodic back-and-forth movement with stick-slip are similar to Figs. 2(c) and 2(d). The trajectories for zigzag movement with stick-slip and double-period back-and-forth motion are shown in Figs. 4(b) and 4(c). These complex motility patterns are found in the region where $v_p^{(0)}$ is large. Note that Fig. 2(a) shows that complex motility patterns are found in regions with strong contractility. These results suggest that as $v_p^{(0)}$ or $\bar{\chi}$ increase, the cell becomes more polarized and it is less easy to reverse its moving direction.

III. SIMPLIFIED MODEL

To obtain an intuitive physical picture of the complex motility behaviors, especially the origin of the periodic back-and-forth movement, it is helpful to describe the dynamics of the system in terms of a system of ordinary differential equations [25]. To achieve this, a simplified model is constructed. In this model, the adhesion complexes are assumed to appear close to the cell ends only, and a cell close to the rest/moving transition is considered such that the myosin motors are located close to the center of the cell. This simplified model allows the dynamics of the cell to be described by a

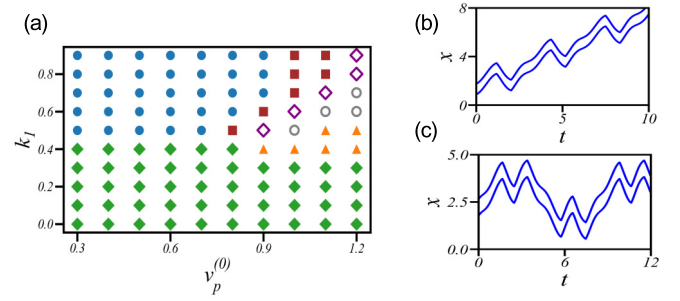


FIG. 4. (a) Phase diagram for the motility behavior in the $v_p^{(0)}$ - k_1 plane. $\bar{\chi} = 14$, $v_p^{(1)} = 0.5$, $v_p^{(2)} = 0.2$. The cells show the following motility behaviors: constant velocity motion (green diamonds), periodic back-and-forth movement (blue circles), stick-slip movement (orange triangles), periodic back-and-forth movement with stick-slip (empty gray circles), zigzag movement with stick-slip (empty purple diamonds), and double-period back-and-forth motion (brown squares). (b) Zigzag with stick-slip, and (c) double-period back-and-forth movement from the active gel model with $K = 100$, $\bar{\chi} = 14$, $k_{\text{on}} = 6.0$, $k_0 = 3.0$, $v_p^{(1)} = 0.5$, $v_p^{(2)} = 0.2$. In (a), $v_p^{(0)} = 1.2$, $k_1 = 0.9$; in (b), $v_p^{(0)} = 1.1$, $k_1 = 0.9$. The blue curves represent the trajectories of the cell ends.

few degrees of freedom, and it becomes possible to study the physical mechanism of autonomous cell polarity change analytically. In this section, we present the basic ideas for constructing our simplified model. Details of the derivations are presented in Appendix C.

Let N_f (N_b) be the total number of adhesion complexes close to l_+ (l_-); it is convenient to introduce $N = N_f + N_b$ and $\Delta N = N_f - N_b$ as ΔN describes the spatial polarization of adhesion complex distribution. With this simplification, the simplified model allows more general forms of mechanosensitivity for the adhesion complexes than our active gel model. Furthermore, the flow field in the cell can be solved as a function of the distribution of myosin motors [Eq. (C6)]. By substituting the flow field into the advection term of the myosin evolution equation, the evolution equation for myosin density becomes a nonlocal integral-differential equation [Eq. (C7)]. According to the discussion in the previous section, the actin polymerization rates are functions of the velocity of the cell and the length of the cell; i.e., $v_p^\pm = v_p^\pm(dl_\pm dt, L)$. Thus the equation for V_{cell} [Eq. (C8)] and the evolution equation for L [Eq. (C9)] can be obtained from v_p^\pm and the flow velocity at l_\pm .

Further simplification can be made by focusing on slow-moving cells, in which the maximum myosin motor density is close to the center of the cell. In this regime, the stress and flow in the cell can be expressed in terms of the moments of the myosin density. For simplicity, we introduce the monopole C_{tot} and dipole y_c of the myosin motor distribution; higher moments are approximated by powers of y_c .

To express the velocity of the cell V_{cell} and the evolution of cell length dL/dt in terms of variables like C_{tot} , y_c , N , and ΔN , the flow velocity at l_\pm is expressed in terms of N , ΔN , and y_c . Let $v_p^\pm \equiv v_p \pm \Delta v_p/2$, where Δv_p (v_p) is the contribution to v_p^\pm that is odd (even) under spatial inversion; V_{cell} and dL/dt become functions of v_p , Δv_p , N , L , ΔN , and

y_c , as shown in Eqs. (C12) and (C14). Since v_p and Δv_p are functions of L , dL/dt , and V_{cell} , our remaining task is to derive the evolution equations for N , ΔN , and y_c .

Unlike our active gel model, in our simplified model, we do not assume any specific force dependencies of the evolution equations for N_f (N_b). Using the assumption that the adhesion complexes are located near the cell ends and the evolutions of N_f , N_b are functions of $|v|$ and $\partial_x v$, for a slow-moving cell, symmetry analysis discussed in Appendix C 5 leads to the following evolution equations of N and ΔN ,

$$\begin{aligned} \frac{dN}{dt} &= (2k_{\text{on}}^{(0)} - k_{\text{off}}^{(0)} N) - k_{\text{off}}^{(1)} y_c \Delta N - k_{\text{off}}^{(\Delta)} \Delta N^2, \\ \frac{d\Delta N}{dt} &= -(k_{\text{off}}^{(0)} + k_{\text{on}}^{(\Delta)} + k_{\text{off}}^{(\Delta)} N) \Delta N - (-k_{\text{on}}^{(1)} + k_{\text{off}}^{(1)} N) y_c. \end{aligned} \quad (8)$$

In principle, the coefficients in the above equations depend on N and L . The y_c -dependent term in $d\Delta N/dt$ indicates that to agree with the experimental observations of adherent cells, one should have $k_{\text{on}}^{(1)} + k_{\text{off}}^{(1)} N > 0$ such that the number of adhesion complexes at the cell end farther from (closer to) the center of the myosin distribution tends to increase (decrease).

The evolution equation for y_c for a slow-moving cell can be derived from the evolution equation of myosin density. In principle, the evolution of the moments of the myosin distribution should depend on higher moments; the resulting coupled equations can only be solved by truncating at some order. In our simplified model, the m th moment of the myosin distribution is approximated by y_c^m , and the resulting evolution of y_c takes the form

$$\frac{dy_c}{dt} = -\Gamma [-(\tilde{\chi} - \tilde{\chi}_c) y_c - a_{\Delta N} \Delta N + a_3 y_c^3]. \quad (9)$$

The coefficients Γ , $\tilde{\chi}_c$, $a_{\Delta N}$, and a_3 are positive, and they depend on L and N . This equation tells us that under sufficiently strong contractility, y_c becomes nonzero as the distribution of myosin motors is spontaneously polarized. Furthermore, the term that contains ΔN tends to drive myosin motors toward the cell end with more adhesion complexes. One can imagine this as an attraction that adhesion complexes at the cell ends exert on the myosin motors.

The simplified model suggests that the dynamics of slow-moving cells with mechanosensitive adhesion complexes can be described by a few variables. Although the final system of equations is derived by assuming the cytoplasm to be a contractile gel, the simplified model can also be regarded as a general model for slow-moving cells because it can be constructed from symmetry considerations alone.

Analytical study of the bifurcation from a cell at rest, i.e., $y_c = 0$, $\Delta N = 0$, to a cell in motion for the simplified model can be carried out in the limit of large K , i.e., $L \approx L_0$. In this limit, all the coefficients in Eqs. (8) and (9) depend only on N . Since N is not essential in determining the polarity of the cell, we neglect this N dependence and treat all coefficients as constants. As one can see from Eq. (C26), solutions with time-independent nonzero ΔN and y_c correspond to a cell moving at a constant velocity; solutions with time-periodic ΔN and y_c are stick-slip (periodic back-and-forth) movement if the time averages of ΔN and y_c are nonzero (zero). The linear

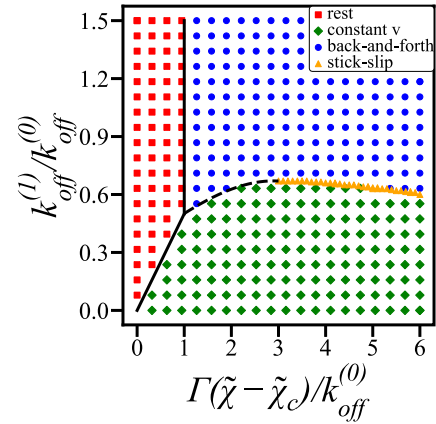


FIG. 5. Phase diagram for the motility behavior predicted by the simplified model with $k_{\text{off}}^{\Delta} = 0$. The following motility patterns are found: a cell at rest (red squares), a cell moving at constant velocity (green diamonds), a cell performing stick-slip movement (orange triangles), a cell performing back-and-forth movement with stick-slip (at $k_{\text{off}}^{(1)}/k_{\text{off}}^{(0)}$ slightly greater than those orange triangles, so that we cannot show this), and a cell performing periodic back-and-forth movement (blue circles). The boundary between the rest and constant velocity movement is Eq. (C29). The boundary between the rest and periodic back-and-forth movement states is Eq. (C31).

stability analysis of the rest state shows that as the contractility increases, a cell at rest starts to move as the system undergoes a bifurcation, and the moving state is the constant-velocity state when $k_{\text{off}}^{(1)}$ is small; when $k_{\text{off}}^{(1)}$ is sufficiently large, the bifurcation leads to a periodic back-and-forth moving state.

Figure 5 shows that the model Eqs. (8) and (9) with constant coefficients exhibit a motility phase diagram qualitatively similar to the numerical solutions of our active gel model. The minor differences come from those simplifications made when constructing the simplified model, as, for example, assuming a constant cell length should affect the detailed shape of the phase boundaries. Furthermore, how the symmetry properties and the couplings of the key driving variables lead to the observed cell motion can be seen from the simplified model. For example, from Eq. (8), ΔN tends to increase when y_c is sufficiently negative, and Eq. (9) states that y_c tends to move toward the cell end with more adhesion complexes. Therefore, at sufficiently large $k_{\text{off}}^{(1)}$, the number of adhesion complexes in the leading end of a moving cell increases sufficiently fast such that at some point, the myosins are pulled to the other half of the cell, reversing the sign of y_c , then reversing the sign of ΔN , and eventually the direction of cell motion is reversed. This is how a cell with highly mechanosensitive adhesion complexes exhibits periodic back-and-forth movement, as illustrated in Fig. 6(a). On the other hand, as shown in Fig. 6(b), $y_c(t)$ and $\Delta N(t)$ in a cell that undergoes stick-slip movement have nonzero time-average values, and they oscillate with similar phase relations as a cell undergoes periodic back-and-forth movement. This is because the mechanosensitivity of the adhesion complexes is sufficiently strong to induce an oscillation of ΔN and y_c , but not sufficiently strong to change the polarity of the cell. Figures 6(c) and 6(d) show that in our active gel mode, $y_c(t)$ and $\Delta N(t)$ (defined as the difference of the total number of

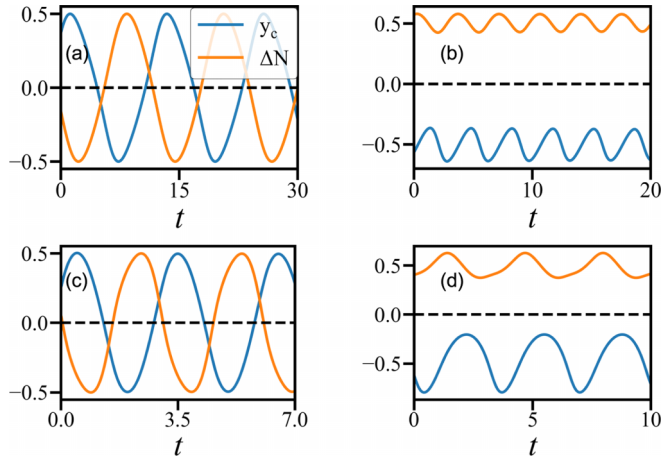


FIG. 6. (a), (b): Normalized $y_c(t)$ and $\Delta N(t)$ in the simplified model with $k_{\text{on}}/k_{\text{off}}^{(0)} = 1$, $a_{\Delta N} = 1$, and $a_3 = 1$. In (a), $k_{\text{off}}^{(1)}/k_{\text{off}}^{(0)} = 0.6$, $\Gamma(\bar{\chi} - \bar{\chi}_c)/k_{\text{off}}^{(0)} = 1.2$; in (b), $k_{\text{off}}^{(1)}/k_{\text{off}}^{(0)} = 0.62$, $\Gamma(\bar{\chi} - \bar{\chi}_c)/k_{\text{off}}^{(0)} = 5.5$. (c), (d): Normalized $y_c(t)$ and $\Delta N(t)$ in the active gel model with $K = 100$, $\tilde{\xi} = 1/3$, $k_{\text{on}} = 6$, $k_0 = 3$, $v_p^{(0)} = 0.2$, $v_p^{(1)} = 0.5$, $v_p^{(2)} = 2$. In (c), $k_1 = 0.55$, $\bar{\chi} = 16$; in (d), $k_1 = 0.1$, $\bar{\chi} = 18$. The cells in (a) and (c) perform oscillatory back-and-forth movement, and the cells in (b) and (d) perform stick-slip movement.

adhesion complexes in the leading and trailing halves of the cell in the numerical simulations) behave similarly to the simplified model; this further indicates that the aforementioned physical picture for the origin of time-periodic motility patterns is general.

IV. DISCUSSION

In this article, we present two models to study how mechanosensitive adhesion complexes affect the motility patterns of a cell. Although these two models are related, they have different assumptions and approximations. This allows us to study the same system from different viewpoints. The fact that both models show similar cell motility behaviors suggests that the underlying mechanisms are not sensitive to the differences in these two models.

We find that a cell with highly mechanosensitive adhesion complexes can exhibit periodic back-and-forth movement similar to what was observed in zyxin-depleted cells in a collagen matrix. Since zyxin proteins act as mechanosensors in mature adhesion complexes [26], the difference in the mechanosensitivity of the adhesion complexes in zyxin-depleted and wild-type cells could be the origin of the periodic back-and-forth movement observed in [5]. Future experiments can be designed to examine this prediction. Our study also suggests that, besides rest, constant-velocity motion, stick-slip movement, and back-and-forth movement, in general, more complex one-dimensional cell motility behaviors can be found, and these complex cell motility behaviors appear in regimes with strong contractility or high actin polymerization velocity, like stick-slip motion.

When modeling the association/dissociation dynamics of the adhesion complexes, information from experimental observations is used very differently. In the active gel model, the association rate of the adhesion complexes is constant, and the dissociation rate decreases as the velocity gradient

increases. This special choice is justified by the resulting spatial distribution of adhesion complexes in the numerical solutions. On the other hand, the simplified model assumes that adhesion complexes only appear near the cell ends, as observed experimentally. This allows our simplified model to describe more general force dependence in the evolution of the number of adhesion complexes. We find that for the cell to have more adhesion complexes near the leading cell end, one should have $-k_{\text{on}}^{(1)} + k_{\text{off}}^{(1)}N > 0$. Note that if we loosely regard N_f and N_b as the total number of adhesion complexes in the two halves of the cell in the active gel model, our active gel model should behave similarly to a simplified model with $k_{\text{on}}^{(1)} = 0$ and $k_{\text{off}}^{(1)} > 0$. This helps us to understand why our active gel model can produce reasonable spatial distributions of adhesion complexes.

Another place where information from experimental observation is important is the actin polymerization velocity in our models. To have actin polymerization at the cell ends regulated by cell length and cell motion, like what happens in real cells, our active gel model introduces coefficients $v_p^{(0)}$, $v_p^{(1)}$, and $v_p^{(2)}$. In the numerical studies, the value of the coefficient $v_p^{(1)}$, which characterizes the effect of cell length restoring force on actin polymerization, is chosen to be consistent with experimental observations. On the other hand, we report how the overall actin polymerization ability $v_p^{(0)}$ affects the cell motility pattern. Although the numerical solutions of the active gel model do not explore whether the symmetry-breaking coefficient $v_p^{(2)}$ plays a significant role in determining the motility behavior of the cell, in our simplified model, the equation for cell velocity Eq. (C26) shows that when the symmetry-breaking part of the actin polymerization velocity Δv_p is a nonlinear function of V_{cell} , polymerization-induced spontaneous cell polarization, or bistability, can happen. Thus, while so far we restrict our attention to the case when polymerization-induced spontaneous cell polarization does not happen, further research on the roles played by polarized actin polymerization in complex cell motility behaviors is needed.

Our models focus on the effect of spatial distributions of adhesion complexes and myosin motors on cell motility patterns. Our assumption of the fast turnover of myosin motors neglected the possible effects of finite myosin turnover time. Although such an effect has not been considered in most cell motility models, it is interesting to see its relation with complex cell motility patterns, as models of active matter with turnover have been shown to generate spontaneous oscillations that are related to observations in other biological active matter systems [27]. Finally, it is important to note that although the physical mechanisms for symmetry-breaking transitions, such as rest/periodic back-and-forth transition and rest/constant-velocity transition, can be understood from the dynamics of y_c and ΔN , it would be an interesting future work [28] to study how other important physical observables, such as the multipoles of the traction force [29,30], behave in cells with different moving patterns.

ACKNOWLEDGMENTS

H.-Y.C. thanks Prof. Jasnow (University of Pittsburgh) for stimulating discussions and encouragement in the early stage

of this work. H.-Y.C. is supported by the Ministry of Science and Technology, Taiwan (MOST 108-2112-M-008-016). The authors also acknowledge support from the National Center for Theoretical Sciences, Taiwan.

APPENDIX A: CHEMICAL POTENTIAL OF AN ADHESION COMPLEX

Experimentally, the association/dissociation of an adhesion complex shows nontrivial force dependence. Only when the force per linker is within a specific range does an adhesion complex grow to a characteristic size $l_a \sim O(\mu\text{m})$ [14]. The physical mechanism behind this behavior has been under intensive theoretical study in recent decades [12]. Since our main focus is how mechanosensitive adhesion complexes induce complex cell motility behaviors, we will not assume detailed molecular mechanisms for the force dependence of the growth/dissociation of adhesion complexes. Instead, in this Appendix, thermodynamic arguments similar to [15] are applied to analyze the chemical potential of a mechanosensitive adhesion complex.

Let us model an adhesion complex as an elastic object adhered to the substrate. In the presence of the flow of the active gel, it experiences total force f_a and a tension γ . Its internal energy is

$$u_a = Ts + \mu_a + \gamma \delta l, \quad (\text{A1})$$

where T is the temperature of the environment and s is the entropy. The chemical potential μ_a of the adhesion complex depends on the total force f_a acting on the adhesion complex. The last term is the elastic energy of the adhesion complex; δl is the change of the length l_a of the adhesion complex due to the tension γ . Since the linkers provide the anchorage, we assume that the molecules in the adhesion complex do not flow with the cytoplasm. Therefore, f_a is the total drag force due to the flow of cytoplasm; it tries to pull the adhesion complex away from the substrate. That is, $f_a = \xi_a \int v(x, t) dx \approx \xi_a l_a v$, where v is the average flow field at the adhesion complex, the integral is performed over the adhesion complex, and $\xi_a l_a = \alpha$ is the drag coefficient in Eq. (1) of the main text. On the other hand, when $v(x, t)$ is not uniform in space, the adhesion complex also experiences a tension $\gamma \sim \partial_x v$ that tries to change its linear dimension, where $\partial_x v$ is the average flow gradient at the adhesion complex. From Eq. (A1), the following relation is obtained:

$$\frac{\partial \mu_a}{\partial \gamma} = -\delta l. \quad (\text{A2})$$

Since δl and γ have the same sign, this equation tells us that μ_a decreases as $\partial_x v$ increases.

When the association/dissociation of the adhesion complexes is completely driven by the change of chemical potential, to have the force-dependent adhesion complex growth, μ_a should be small for a range of v . Furthermore, from Eq. (A2), adhesion complexes are favored in regions where $\partial_x v$ is large because the chemical potential is lower.

TABLE I. Definitions of physical parameters and characteristic quantities in our model.

Physical meaning	Symbol
effective drag coefficient	$\xi_{\text{eff}} = \xi + \alpha k_{on}/k_0$
unit length	$l_0 = \sqrt{\eta/\xi_{\text{eff}}}$
unit time	$t_0 = \eta/\xi_{\text{eff}}D$
unit stress	$\sigma_0 = \xi_{\text{eff}}D$
unit myosin motors concentration	$c_0 = \frac{M}{\sqrt{\eta/\xi_{\text{eff}}}}$
unit density of cell-substrate bonds	$n_0 = \xi/\alpha$

APPENDIX B: DIMENSIONLESS EQUATIONS AND PARAMETERS; NUMERICAL METHOD

In the dimensionless form, the equations of motion are

$$\frac{\partial^2 v}{\partial x^2} - \xi(1 + n_b)v = -\tilde{\chi} \frac{\partial c}{\partial x}, \quad (\text{B1})$$

$$\frac{\partial c}{\partial t} = \frac{\partial^2 c}{\partial x^2} - \frac{\partial(cv)}{\partial x}, \quad (\text{B2})$$

$$\frac{\partial n_b}{\partial t} = -\bar{k}_0 e^{-\bar{k}_1 \partial_x v} n_b + \bar{k}_{on}. \quad (\text{B3})$$

The boundary conditions are

$$\frac{dl_{\pm}}{dt} = [v]_{l_{\pm}} \pm v_p^{\pm}, \quad (\text{B4})$$

$$\left[c \left(v - \frac{dl}{dt} \right) - \frac{\partial c}{\partial x} \right]_{l_{\pm}} = 0, \quad (\text{B5})$$

$$\sigma_{\pm} = -K(L - L_0) = \left[\frac{\partial v}{\partial x} \right]_{l_{\pm}} + \tilde{\chi} c_{l_{\pm}}. \quad (\text{B6})$$

Here, all variables and x, t are dimensionless. The definitions of the parameters and important physical quantities are listed in Table I. The dimensionless parameters in our model are listed in Table II. Notice that, for simplicity, in the figures and figure captions, we drop the overbars from the dimensionless rates.

In our numerical scheme, each iteration updates all dynamical variables by integrating the evolution equations over a small time interval Δt with a finite-difference method. First, $[v]_{l_{\pm}}$ and v_p^{\pm} from the previous iteration were substituted into Eq. (B4) to obtain the new positions of the cell ends. The densities of the adhesion complexes and myosin motors are updated from the flow field of the previous iteration by integrating the evolution Eq. (B3) of n_b and the myosin advection-diffusion Eq. (B2). The force balance Eq. (B1) with the updated bond density and myosin concentration is then solved to obtain the new flow field.

The numerics were carried out by dividing the cell into $N_x = 100$ segments and approximating the spatial derivatives by the finite-difference method with the size of a time step $\Delta t = 10^{-6}$. The typical material parameters are $D \sim 0.1\text{--}1 \mu\text{m}^2/\text{s}$ for proteins in a cell [31], and the length of a cell is in the range $10\text{--}100 \mu\text{m}$. From the traction force measurement of a cell, the typical drag force that a cell exerts on the substrate is of the order of 10 nN [32], and the typical magnitude of cytoplasmic flow $\sim 10^2 \text{ nm/s}$. The effective

TABLE II. Definitions of dimensionless parameters in our model.

Physical meaning	Symbol	Magnitude
unbinding rate	$\bar{k}_0 = t_0 k_0$	3
coefficient for strain-rate-dependent unbinding	$\bar{k}_1 = k_1/t_0$	$\lesssim O(1)$
binding rate	$\bar{k}_{\text{on}} = k_{\text{on}} t_0/n_0$	6
base actin polymerization speed	$\bar{v}_p^{(0)} = v_p^{(0)} l_0/t_0$	$\lesssim O(1)$
coefficient for stress-dependent actin polymerization	$\bar{v}_p^{(1)} = v_p^{(1)} l_0$	0.5
coefficient for cell polarization effect on actin polymerization	$\bar{v}_p^{(2)} = v_p^{(2)} t_0/l_0$	2
contractility	$\bar{\chi} = c_0 \chi/\sigma_0$	$\sim O(10)$
cell elastic constant	$K = \gamma l_0/\sigma_0$	100
drag coefficient	$\bar{\xi} = \xi/(\xi + \alpha k_{\text{on}}/k_0)$	1/3

drag coefficient ξ_{eff} can be estimated by dividing traction force per unit length by typical cytoplasmic flow speed. The result is $\xi_{\text{eff}} \sim 10^3\text{--}10^4$ kg/(m s). The one-dimensional viscosity of the actin gel can be estimated by multiplying the three-dimensional viscosity of the actin gel $\sim 10^4$ Pa s by the cross-sectional area A_0 of a cell perpendicular to the moving direction. The cross section of a cell has a height of a few hundred nanometers and a width of a few tens of microns. This leads to $\eta \sim 10^{-7}$ kg m/s, and the order of magnitude of our unit length

$$l_0 = \sqrt{\frac{\eta}{\xi_{\text{eff}}}} \sim 10 \mu\text{m}. \quad (\text{B7})$$

Since this is close to the length of a cell, in our numerical studies we conveniently choose the dimensionless cell natural length to be unity. The unit time is roughly [33]

$$t_0 = \frac{\eta}{\xi_{\text{eff}} D} \sim 10^3 \text{ s}, \quad (\text{B8})$$

and the unit stress

$$\sigma_0 = \xi_{\text{eff}} D \sim 10^{-9} \text{ to } 10^{-10} \text{ kg m/s}^2. \quad (\text{B9})$$

Now we can estimate the magnitudes of the dimensionless parameters listed in Table II. The typical speed of a crawling cell is about a few cell body lengths per hour [34]; therefore the base active polymerization speed in the numerics is in the range

$$\bar{v}_p^{(0)} \lesssim O(1). \quad (\text{B10})$$

The cell-length-dependent actin polymerization parameter $v_p^{(1)}$ comes from the free energy cost of actin polymerization against cell-length restoring force. Because adding a new actin monomer to the plus end of an actin filament effectively pushes the cell membrane by a distance a_0 of the order of a nanometer, $v_p^{(1)}(L - L_0)$ in Eq. (4) is W_a , the work done by adding one actin monomer to an actin filament at the cell end, divided by $k_B T$, i.e., the thermal energy. W_a is the average cell-length restoring force on each filament times a_0 . Since the average distance between two actin filaments close to a cell end d_0 is a few tens of nanometers [35],

$$\bar{v}_p^{(1)} \sim \frac{\gamma l_0 a_0}{(A_0/d_0^2) k_B T} \sim 0.1\text{--}1, \quad (\text{B11})$$

in our numerical studies, we choose $\bar{v}_p^{(1)} = 0.5$. From Eq. (4), the effect of the asymmetric actin polymerization parameter $\bar{v}_p^{(2)}$ is significant when $\bar{v}_p^{(2)}$ is small. In this limit, the actin polymerization speed at the cell leading end is enhanced by a factor ~ 2 , and the actin polymerization speed at the trailing end becomes almost zero. In the numerics, we choose $\bar{v}_p^{(2)}$ to be of order unity so that the asymmetry of actin protrusion in a typical moving cell is neither negligible nor extreme.

Next, we discuss the rates related to the association/dissociation of adhesion complexes. k_0 is the dissociation rate of a mature focal adhesion; its typical value is $\sim 0.1\text{--}1/\text{min}$ [36]. Thus we chose

$$\bar{k}_0 = 3. \quad (\text{B12})$$

In the dimensionless force balance Eq. (B1), n_b denotes the contribution of adhesion complexes to the local cell-substrate drag relative to the rest of the cell-substrate interface. Similarly to a previous numerical model for cell crawling [37], we choose our parameters such that the average of n_b over the cell is in the range 1–10; this is achieved by choosing

$$\bar{k}_{\text{on}} = 6, \quad (\text{B13})$$

and varying the parameter \bar{k}_1 in the numerics within the range

$$\bar{k}_1 \lesssim O(1). \quad (\text{B14})$$

From the measurement of the elastic constant of living cells in Ref. [32], the Young's modulus of a cell is $Y \sim 500$ Pa. Multiplying Y by the thickness of a cell, we obtain $\gamma \sim 10^{-4}$ kg/s². This leads to the dimensionless cell elastic constant

$$K = \frac{\gamma l_0}{\sigma_0} \sim O(10\text{--}100). \quad (\text{B15})$$

Following previous studies on the actin gel model of cell motility [11], in our numerical studies we choose $K = 100$. We choose $\bar{\xi} = 1/3$ so that the resulting drag force in the cell is of the same order as [11]. Since the dimensionless contractility $\bar{\chi} = \chi c_0/\sigma_0$ is a parameter that we vary in the numerics, we choose the dimensionless total number of myosin motors in the cell to be $c_0 L_0 = 1$ for simplicity. As a result, the rest/moving transitions happen when $\bar{\chi}$ is of the order of 10, similarly to [11].

The magnitudes of all the dimensionless parameters are summarized in Table II.

APPENDIX C: DERIVATION OF THE SIMPLIFIED MODEL

Since in the experiments, the adhesion complexes are distributed close to the cell ends, our derivation of the simplified model begins with the assumption

$$n_b(x, t) = N_f \delta(x - x_f) + N_b \delta(x - x_b), \quad (\text{C1})$$

where $x_f = l_+ - \epsilon$, $x_b = l_- + \epsilon$, and ϵ is a very small length.

1. Stress field and flow field

Because there are no adhesion complexes in $x_b < x < x_f$, the dimensionless momentum equation in this region is

$$\partial_x \sigma = \tilde{\xi} v, \quad \sigma = \partial_x v + \tilde{\chi} c, \quad x_b < x < x_f. \quad (\text{C2})$$

Integrating the full momentum equation from $l_{+(-)}$ to $x_{f(b)}$, we find

$$\sigma_f = -K(l - l_0) - \tilde{\xi} N_f v_f, \quad \sigma_b = -K(l - l_0) + \tilde{\xi} N_b v_b. \quad (\text{C3})$$

Here $v_f = v(x_f, t) \approx dl_+/dt - v_p^+$, and $v_b = v(x_b, t) \approx dl_-/dt + v_p^-$. The resulting solution of the mechanical stress

in the cell is [13]

$$\begin{aligned} \sigma(x, t) = & \sigma_f \frac{\sinh[\tilde{\xi}^{1/2}(x - x_b)]}{\sinh[\tilde{\xi}^{1/2}(x_f - x_b)]} + \sigma_b \frac{\sinh[\tilde{\xi}^{1/2}(x_f - x)]}{\sinh[\tilde{\xi}^{1/2}(x_f - x_b)]} \\ & + \tilde{\chi} \tilde{\xi}^{1/2} \int_{x_b}^{x_f} G(x, x') c(x', t) dx', \end{aligned} \quad (\text{C4})$$

where

$$\begin{aligned} G(x, x') = & \frac{\sinh[\tilde{\xi}^{1/2}(x_f - x)] \sinh[\tilde{\xi}^{1/2}(x' - x_b)]}{\sinh[\tilde{\xi}^{1/2}(x_f - x_b)]} \\ & - \Theta(x' - x) \sinh[\tilde{\xi}^{1/2}(x' - x)]; \end{aligned} \quad (\text{C5})$$

$\Theta(x)$ is the Heaviside step function. This leads to the following expression for the flow field,

$$\begin{aligned} v(x, t) = & \frac{1}{\tilde{\xi}^{1/2}} \left\{ \sigma_f \frac{\cosh[\tilde{\xi}^{1/2}(x - x_b)]}{\sinh[\tilde{\xi}^{1/2}(x_f - x_b)]} \right. \\ & - \sigma_b \frac{\cosh[\tilde{\xi}^{1/2}(x_f - x)]}{\sinh[\tilde{\xi}^{1/2}(x_f - x_b)]} \\ & \left. + \tilde{\chi} \int_{x_b}^{x_f} \partial_x G(x, x') c(x', t) dx' \right\}. \end{aligned} \quad (\text{C6})$$

2. Myosin concentration

Substituting Eq. (C6) into the advection-diffusion for myosin concentration, one obtains an equation that does not explicitly depend on the velocity field:

$$\partial_t c(x, t) = D \partial_x^2 c - \frac{1}{\tilde{\xi}^{1/2}} \partial_x \left\{ \left[\sigma_f \frac{\cosh[\tilde{\xi}^{1/2}(x - x_b)]}{\sinh[\tilde{\xi}^{1/2}(x_f - x_b)]} - \sigma_b \frac{\cosh[\tilde{\xi}^{1/2}(x_f - x)]}{\sinh[\tilde{\xi}^{1/2}(x_f - x_b)]} \right] c(x, t) + \tilde{\chi} \int_{x_b}^{x_f} c(x, t) \partial_x G(x, x') c(x', t) dx' \right\}. \quad (\text{C7})$$

3. Velocity and length of the cell

The velocity of the cell $V_{\text{cell}} = \frac{1}{2} \left(\frac{dl_+}{dt} + \frac{dl_-}{dt} \right)$ is

$$\begin{aligned} V_{\text{cell}} = & \frac{1}{2\tilde{\xi}^{1/2}} \frac{\cosh(\tilde{\xi}^{1/2}L) + 1}{\sinh(\tilde{\xi}^{1/2}L)} (\sigma_f - \sigma_b) + \frac{\tilde{\chi}}{2} \int_{x_b}^{x_f} \frac{\sinh[\tilde{\xi}^{1/2}(x_f - x')] - \sinh[\tilde{\xi}^{1/2}(x' - x_b)]}{\sinh(\tilde{\xi}^{1/2}L)} c(x', t) dx' \\ & + \frac{v_p^+ - v_p^-}{2}. \end{aligned} \quad (\text{C8})$$

The evolution of the length of the cell $\frac{dL}{dt} = \frac{dl_+}{dt} - \frac{dl_-}{dt}$ obeys

$$\begin{aligned} \frac{dL}{dt} = & \frac{1}{\tilde{\xi}^{1/2}} \frac{\cosh(\tilde{\xi}^{1/2}L) - 1}{\sinh(\tilde{\xi}^{1/2}L)} (\sigma_f + \sigma_b) - \tilde{\chi} \int_{x_b}^{x_f} \frac{\sinh[\tilde{\xi}^{1/2}(x_f - x')] + \sinh[\tilde{\xi}^{1/2}(x' - x_b)]}{\sinh(\tilde{\xi}^{1/2}L)} c(x', t) dx' \\ & + (v_p^+ + v_p^-). \end{aligned} \quad (\text{C9})$$

4. Symmetry-related variables

It is helpful to introduce the following variables:

$$\begin{aligned} N &= N_f + N_b, \quad \Delta N = N_f - N_b, \\ v_p &= \frac{v_p^+ + v_p^-}{2}, \quad \Delta v_p = v_p^+ - v_p^-, \\ \sigma_S &= \frac{\sigma_f + \sigma_b}{2} = -K(L - L_0) - \frac{\tilde{\xi}}{2} \left[N \left(\frac{dL/dt}{2} - v_p \right) + \Delta N \left(V_{\text{cell}} - \frac{\Delta v_p}{2} \right) \right], \\ \sigma_A &= \frac{\sigma_f - \sigma_b}{2} = -\frac{\tilde{\xi}}{2} \left[N \left(V_{\text{cell}} - \frac{\Delta v_p}{2} \right) + \Delta N \left(\frac{dL/dt}{2} - v_p \right) \right], \end{aligned} \quad (\text{C10})$$

and

$$y = x - \frac{L_+ + L_-}{2}, \quad \left(-\frac{L}{2} \leq y \leq \frac{L}{2}\right). \quad (\text{C11})$$

Here dL/dt , N , v_p , and σ_S are symmetric under spatial inversion ($y \rightarrow -y$), while V_{cell} , ΔN , Δv_p , and σ_A are antisymmetric under spatial inversion.

Next, we show that the velocity of the cell V_{cell} and the evolution of the length of the cell dL/dt can be expressed in terms of variables in Eq. (C10). To achieve this, we focus on the regime close to rest-moving transitions. In this regime, we can assume that the myosin motors are weakly polarized. As a result, the zeroth and first moments of the myosin density distribution dominate the contribution of contractility to the cell motility behaviors [Eq. (C8)].

Because only the part of $c(y)$ that is antisymmetric under $y \rightarrow -y$ contributes to the $\tilde{\chi}$ -dependent term of Eq. (C8), and for a slow-crawling cell this part is significant only in the small- $|y|$ region, therefore by expanding the $\tilde{\chi}$ -dependent term of V_{cell} to the leading order in y , and using Eq. (C10), we obtain

$$V_{\text{cell}} = \frac{\Delta v_p}{2} - \tilde{\xi}^{1/2} \left[1 + \frac{\tilde{\xi}^{1/2} \cosh(\tilde{\xi}^{1/2} L) + 1}{2 \sinh(\tilde{\xi}^{1/2} L)} N \right]^{-1} \left[\frac{1 \cosh(\tilde{\xi}^{1/2} L) + 1}{2 \sinh(\tilde{\xi}^{1/2} L)} \left(\frac{1}{2} \frac{dL}{dt} - v_p \right) \Delta N + \tilde{\chi} \frac{\cosh(\tilde{\xi}^{1/2} L/2)}{\sinh(\tilde{\xi}^{1/2} L)} y_c + \dots \right], \quad (\text{C12})$$

where

$$y_c \equiv \int_{-L/2}^{L/2} y c(y, t) dy \quad (\text{C13})$$

is the first moment of myosin distribution, and “...” represents higher-order terms in this expansion. This expression tells us that V_{cell} is nonzero when ΔN (asymmetry in the distribution of adhesion complexes) or y_c (asymmetry in the distribution of myosin motors) is nonzero. Note that, in principle, Δv_p is a nonlinear function of V_{cell} ; this indicates that Eq. (C12) can describe cell movement induced by spontaneous symmetry breaking in actin polymerization velocity. Although studying this possible situation with our simplified model is not the main focus of this study, as pointed out in Sec. IV, it is a future research direction.

Similar calculation leads to the following expression for the evolution of the length of the cell:

$$\begin{aligned} \frac{dL}{dt} = & 2v_p + \left[1 + \frac{\tilde{\xi}^{1/2} \cosh(\tilde{\xi}^{1/2} L) - 1}{2 \sinh(\tilde{\xi}^{1/2} L)} N \right]^{-1} \\ & \times \left\{ \tilde{\xi}^{-1/2} \frac{\cosh(\tilde{\xi}^{1/2} L) - 1}{\sinh(\tilde{\xi}^{1/2} L)} \left[-2K(L - L_0) + \Delta N \left(V_{\text{cell}} - \frac{\Delta v_p}{2} \right) \right] - 2\tilde{\chi} \frac{\sinh(\tilde{\xi}^{1/2} L/2)}{\sinh(\tilde{\xi}^{1/2} L)} C_{\text{tot}} + \dots \right\}, \quad (\text{C14}) \end{aligned}$$

where

$$C_{\text{tot}} \equiv \int_{-L/2}^{L/2} c(y, t) dy \equiv 1 \quad (\text{C15})$$

is the total amount of myosin motors in the cell, which is unity in our dimensionless expression. Note that all terms on the right-hand side of dL/dt are even under $y \rightarrow -y$.

5. Further simplifications

As discussed in the main text, the actin polymerization velocity v_p^\pm can be modeled as functions of L and dl_\pm/dt [Eq. (4)]. Hence, from Eqs. (C12) and (C14), V_{cell} and dL/dt are functions of L , N , ΔN , and y_c . If a set of evolution equations for N , ΔN , and y_c can be derived, a few variables can specify the cell's dynamics. This subsection explains how this is done.

It is convenient to introduce

$$c_S(y) = \frac{c(y) + c(-y)}{2}, \quad c_A(y) = \frac{c(y) - c(-y)}{2}, \quad (\text{C16})$$

and

$$v_S(y) = \frac{v(y) - v(-y)}{2}, \quad v_A(y) = \frac{v(y) + v(-y)}{2}. \quad (\text{C17})$$

From Eq. (C6),

$$\begin{aligned} v_S(y) = & v_{S\sigma}(y) \sigma_S + \frac{\tilde{\chi}}{\tilde{\xi}^{1/2}} \int \partial_y G(y, y') c_S(y') dy', \\ v_A(y) = & v_{A\sigma}(y) \sigma_A + \frac{\tilde{\chi}}{\tilde{\xi}^{1/2}} \int \partial_y G(y, y') c_A(y') dy', \quad (\text{C18}) \end{aligned}$$

where $v_{S\sigma}(y)$ and $v_{A\sigma}(y)$ can be obtained by straightforward algebra. From Eqs. (C10), (C12), and (C14), expand $G(y, y')$ around $y' = 0$ and integrate over y' , use the approximation $\int y^m c(y, t) dy \approx y_c^m$ for all m , and σ_S and σ_A can be expressed as

$$\begin{aligned} \sigma_S = & \sigma_{S_0}(L, N) + \sigma_{S_y}(L, N) y_c^2 + \sigma_{S_\Delta}(L, N) \Delta N^2 \\ & + \sigma_{S_{y\Delta}}(L, N) y_c \Delta N + \dots, \\ \sigma_A = & \sigma_{A_y}(L, N) y_c + \sigma_{A_\Delta}(L, N) \Delta N + \dots. \quad (\text{C19}) \end{aligned}$$

The functions of (L, N) in the above equations can be obtained by straightforward algebra. Their detailed expressions are not important for the rest of our analysis. The main point is that, with Eqs. (C18) and (C19), the time derivatives of N , ΔN , and y_c can be expressed in terms of power series of ΔN and y_c .

First, from the evolution equations of N_f and N_b

$$\begin{aligned}\frac{dN_f}{dt} &= k_{\text{on}}^{(f)} - k_{\text{off}}^{(f)} N_f, \\ \frac{dN_b}{dt} &= k_{\text{on}}^{(b)} - k_{\text{off}}^{(b)} N_b,\end{aligned}$$

one can introduce

$$\begin{aligned}\frac{dN}{dt} &= k_{\text{on}}^{(f)} + k_{\text{on}}^{(b)} - \frac{k_{\text{off}}^{(f)} + k_{\text{off}}^{(b)}}{2} N - \frac{k_{\text{off}}^{(f)} - k_{\text{off}}^{(b)}}{2} \Delta N, \\ \frac{d\Delta N}{dt} &= k_{\text{on}}^{(f)} - k_{\text{on}}^{(b)} - \frac{k_{\text{off}}^{(f)} - k_{\text{off}}^{(b)}}{2} N - \frac{k_{\text{off}}^{(f)} + k_{\text{off}}^{(b)}}{2} \Delta N.\end{aligned}\quad (\text{C20})$$

Because of mechanosensitivity, the rates $k_{\text{on}}^{(f)}$, $k_{\text{on}}^{(b)}$, $k_{\text{off}}^{(f)}$, $k_{\text{off}}^{(b)}$ should depend on the magnitude of drag force and stress acting on an adhesion complex. This means that they are functions of $|v|_{y_f, y_b}$ and $[\partial_y v]_{y_f, y_b}$. By symmetry, when $v_A(y) = 0$, we have $k_{\text{on}}^{(f)} = k_{\text{on}}^{(b)}$ and $k_{\text{off}}^{(f)} = k_{\text{off}}^{(b)}$. Therefore both $k_{\text{on}}^{(f)} - k_{\text{on}}^{(b)}$ and $k_{\text{off}}^{(f)} - k_{\text{off}}^{(b)}$ are proportional to v_A for a weakly polarized cell. Since we assume myosin motors are located close to the center of the cell, the $\tilde{\chi}$ -dependent part in Eq. (C18) can be expanded around $y' = 0$. The resulting expression for $v_A(y)$ takes the form

$$v_A(y) = \tilde{\chi} v_{Ay}(y) y_c + v_{A\Delta}(y) \Delta N + \dots,$$

where functions $v_{Ay}(y)$ and $v_{A\Delta}(y)$ can be obtained from straightforward algebra. As a result, we can write

$$\begin{aligned}k_{\text{on}}^{(f)} - k_{\text{on}}^{(b)} &= k_{\text{on}}^{(1)} y_c + k_{\text{on}}^{(\Delta)} \Delta N + \dots, \\ \frac{k_{\text{off}}^{(f)} - k_{\text{off}}^{(b)}}{2} &= k_{\text{off}}^{(1)} y_c + k_{\text{off}}^{(\Delta)} \Delta N + \dots,\end{aligned}\quad (\text{C21})$$

where $k_{\text{on}}^{(1)}$, $k_{\text{on}}^{(\Delta)}$, $k_{\text{off}}^{(1)}$ and $k_{\text{off}}^{(\Delta)}$ depend on N and L only. It can be shown that $k_{\text{off}}^{(1)}$ is always positive, but the sign of $k_{\text{off}}^{(\Delta)}$ depends on $dL/dt - 2v_p(L)$, which may change with time. A similar analysis leads to

$$\begin{aligned}k_{\text{on}}^{(f)} + k_{\text{on}}^{(b)} &= 2k_{\text{on}}^{(0)} + \dots, \\ \frac{k_{\text{off}}^{(f)} + k_{\text{off}}^{(b)}}{2} &= k_{\text{off}}^{(0)} + \dots,\end{aligned}\quad (\text{C22})$$

where $k_{\text{on}}^{(0)}$ and $k_{\text{off}}^{(0)}$ are coefficients which depend on N and L , and \dots are terms of the order y_c^2 , ΔN^2 , and $y_c \Delta N$. Putting Eqs. (C23), (C21), and (C22) together, the evolution equations of N and ΔN obey

$$\begin{aligned}\frac{dN}{dt} &= (2k_{\text{on}}^{(0)} - k_{\text{off}}^{(0)} N) - k_{\text{off}}^{(1)} y_c \Delta N - k_{\text{off}}^{(\Delta)} \Delta N^2, \\ \frac{d\Delta N}{dt} &= -(k_{\text{off}}^{(0)} + k_{\text{on}}^{(\Delta)} + k_{\text{off}}^{(\Delta)} N) \Delta N - (-k_{\text{on}}^{(1)} + k_{\text{off}}^{(1)} N) y_c.\end{aligned}\quad (\text{C23})$$

This is Eq. (8) of the main text.

The evolution of y_c is considered next. From its definition,

$$\begin{aligned}\frac{dy_c}{dt} &= \frac{d}{dt} \int_{x_b}^{x_f} \left(x - \frac{x_f + x_b}{2} \right) c(x, t) dx \\ &= \int x [D\partial_x^2 c - \partial_x(cv)] dx \\ &\quad + \frac{dx_f}{dt} [xc]_{x_f} - \frac{dx_b}{dt} [xc]_{x_b} - \frac{V_{\text{cell}}}{2} C_{\text{tot}} \\ &= - \int (D\partial_y c - cv) dy - \frac{V_{\text{cell}}}{2} C_{\text{tot}}.\end{aligned}$$

To derive the last expression from the second expression, we performed integration by parts and used the boundary conditions for myosin motor density. The first term in the integral of the last expression is a surface term; it is vanishingly small because in a slow-moving cell myosin motors are not presented at the cell ends. By symmetry, the contribution of the second term in the integral of the last expression can be reexpressed in terms of c_S , c_A , v_S , and v_A , and we find

$$\frac{dy_c}{dt} = \int (c_A v_S + c_S v_A) dy - \frac{V_{\text{cell}}}{2} C_{\text{tot}}.\quad (\text{C24})$$

Substitute Eqs. (C18) and (C19) into Eq. (C24), and use the approximation $\int y^m c dy \approx y_c^m$; the resulting evolution equation for y_c takes the form

$$\frac{dy_c}{dt} = -\Gamma [-(\tilde{\chi} - \tilde{\chi}_c) y_c - a_{\Delta N} \Delta N + a_3 y_c^3 + \dots].\quad (\text{C25})$$

Here Γ , $\tilde{\chi}_c$, $a_{\Delta N}$, and a_3 depend on L and N . This is Eq. (9) of the main text. It describes a cell that becomes polarized ($y_c \neq 0$) when $\tilde{\chi}$ is sufficiently large. $a_{\Delta N}$ tells us how nonzero ΔN affects the evolution of y_c , and $a_3 > 0$ such that y_c is always finite.

The above discussion leads to a set of closed equations describing the dynamics of a cell in terms of L , N , ΔN , and y_c .

6. Transitions between different motility behaviors

The set of equations for dN/dt , $d\Delta N/dt$, dy_c/dt , dL/dt , and V_{cell} in the previous subsection are derived by assuming the cytoplasm as a contractile gel. However, it is quite clear that these equations can also be written down by symmetry considerations alone. Since we would like to focus on the physics most relevant to the transitions between different motility behaviors, we take this approach by treating the coefficients in these equations as independent model parameters in the rest of our analysis.

For simplicity, we neglect the L dependencies of all coefficients in our simplified model by considering the large- K regime such that $L \rightarrow L_0$. The N dependencies in $\tilde{\chi}_c$ and $a_{\Delta N}$ are also neglected as they do not change the symmetry of the evolution equation of y_c . This approximation is expected to be suitable for slow-moving cells, where N takes a value close to

$2k_{\text{on}}^{(0)}/k_{\text{off}}^{(0)}$. In this regime,

$$V_{\text{cell}} = \frac{\Delta v_p}{2} + \frac{\xi^{1/2}}{1 + \frac{\xi^{1/2} \cosh(\xi^{1/2} L_0) + 1}{2 \sinh(\xi^{1/2} L_0)}} N$$

$$\times \left\{ \left[\frac{v_p \cosh(\xi^{1/2} L_0) + 1}{2 \sinh^2(\xi^{1/2} L_0)} \right] \Delta N - \left[\tilde{\chi} \frac{\cosh(\xi^{1/2} L_0/2)}{\sinh(\xi^{1/2} L_0)} \right] y_c \right\}$$

$$\equiv \frac{\Delta v_p}{2} + (v_p \lambda_{v1} \Delta N - \tilde{\chi} \lambda_{v2} y_c). \quad (\text{C26})$$

$$y_c = \mp \sqrt{\frac{p_4 + p_1^2 p_2 - \sqrt{(p_4 + p_1^2 p_2)^2 - 4 p_1^2 p_4 (p_2 - p_1 p_3 N_0)}}{2 p_1^2 p_4}},$$

$$\Delta N = -\frac{p_1 N_0}{1 + (p_1 y_c)^2} y_c,$$

$$N = \frac{N_0}{1 - (p_1 y_c)^2}, \quad (\text{C28})$$

where $p_1 = k_{\text{off}}^{(1)}/k_{\text{off}}^{(0)}$, $p_2 = \Gamma(\tilde{\chi} - \tilde{\chi}_c)/k_{\text{off}}^{(0)}$, $p_3 = \Gamma a_{\Delta N}/k_{\text{off}}^{(0)}$, and $p_4 = \Gamma a_3/k_{\text{off}}^{(0)}$. Further checking the linear stability of the rest state shows that the transition from the rest state to the state with constant velocity is a pitchfork bifurcation. On the other hand, the transition from the rest state to the periodic back-and-forth movement is a Hopf bifurcation: Pitchfork bifurcation (rest/constant-velocity transition) happens when

$$\tilde{\chi} = \tilde{\chi}_c + 2a_{\Delta N} \frac{k_{\text{on}}^{(0)} k_{\text{off}}^{(1)}}{(k_{\text{off}}^{(0)})^2} \quad (\text{C29})$$

Here λ_{v1} and λ_{v2} are non-negative parameters. Note that V_{cell} tends to take the same (opposite) sign with ΔN (y_c).

Many interesting features of the system described by Eqs. (C23) and (C25) can be studied analytically. To compare to our active gel model, we choose $k_{\text{on}}^{(f)} = k_{\text{on}}^{(b)} = k_{\text{on}}^{(0)}$ a constant. We also choose $k_{\text{off}}^{(\Delta)} = 0$ because it does not play an important role in the polarization of the cell. The resulting steady-state solutions include the rest-state solution

$$\Delta N = y_c = 0, \quad N = \frac{2k_{\text{on}}^{(0)}}{k_{\text{off}}^{(0)}} \equiv N_0, \quad (\text{C27})$$

and solutions for a cell moving in the $\pm x$ direction with a constant velocity,

and

$$\Gamma(\tilde{\chi} - \tilde{\chi}_c) - k_{\text{off}}^{(0)} < 0. \quad (\text{C30})$$

Hopf bifurcation (rest/back-and-forth-motion transition) occurs when

$$\tilde{\chi} = \tilde{\chi}_c + k_{\text{off}}^{(0)}/\Gamma \quad (\text{C31})$$

and

$$\tilde{\chi} - \left[\tilde{\chi}_c + 2a_{\Delta N} \frac{k_{\text{on}}^{(0)} k_{\text{off}}^{(1)}}{(k_{\text{off}}^{(0)})^2} \right] < 0. \quad (\text{C32})$$

- [1] D. Bray, *Cell Movements*, 2nd ed. (Taylor and Francis, New York, 2001).
- [2] P. T. Yam, C. A. Wilson, L. Ji, B. Hebert, E. L. Barnhart, N. A. Dye, P. W. Wiseman, G. Danuser, and J. A. Theriot, Actin-myosin network reorganization breaks symmetry at the cell rear to spontaneously initiate polarized cell motility, *J. Cell Biol.* **178**, 1207 (2007).
- [3] *Physical Models of Cell Motility*, edited by I. S. Aranson (Springer, Heidelberg, 2016).
- [4] Y. Aratyn-Schaus and M. L. Gardel, Transient frictional slip between integrin and the ECM in focal adhesions under myosin II tension, *Curr. Biol.* **20**, 1145 (2010).
- [5] S. I. Fraley, Y. Feng, A. Giri, G. D. Longmore, and D. Wirtz, Dimensional and temporal controls of three-dimensional cell migration by zyxin and binding partners, *Nat. Commun.* **3**, 719 (2012).
- [6] M. Chabaud *et al.*, Cell migration and antigen capture are antagonistic processes coupled by myosin II in dendritic cells, *Nat. Commun.* **6**, 7526 (2015).
- [7] B. A. Camley, Y. Zhao, B. Li, H. Levine, and W.-J. Rappel, Periodic migration in a physical model of cells on micropatterns, *Phys. Rev. Lett.* **111**, 158102 (2013).
- [8] P. Sens, Stick-slip model for actin-driven cell protrusions, cell protrusions, cell polarization, and crawling, *Proc. Natl. Acad. Sci. USA* **117**, 24670 (2020).
- [9] J. E. Ron, P. Monzo, M. C. Gauthier, R. Voituriez, and N. S. Gov, One-dimensional cell motility patterns, *Phys. Rev. Res.* **2**, 033237 (2020).
- [10] F. Jülicher, K. Kruse, J. Prost, and J.-F. Joanny, Active behavior of the cytoskeleton, *Phys. Rep.* **449**, 3 (2007).
- [11] P. Recho, T. Putelat, and L. Truskinovsky, Contraction-driven cell motility, *Phys. Rev. Lett.* **111**, 108102 (2013).
- [12] U. S. Schwarz and S. A. Safran, Physics of adherent cells, *Rev. Mod. Phys.* **85**, 1327 (2013).
- [13] P. Recho and L. Truskinovsky, Cell locomotion in one dimension, in *Physical Models of Cell Motility* (Springer, Heidelberg, 2016), p. 135.

- [14] A. D. Bershadsky, N. Q. Balaban, and B. Geiger, Adhesion-dependent cell mechanosensitivity, *Annu. Rev. Cell Dev. Biol.* **19**, 677 (2003).
- [15] T. Shemesh, B. Geiger, A. D. Bershadsky, and M. M. Kozlov, Focal adhesions as mechanosensors: A physical mechanism, *Proc. Natl. Acad. Sci. USA* **102**, 12383 (2005).
- [16] J. Aureille, S. F. H. Barnett, I. Arnal, L. Lafanechère, B. C. Low, P. Kanchanawong, A. Mogilner, and A. D. Bershadsky, Focal adhesions are controlled by microtubules through local contractility regulation, *bioRxiv* 2023.04.17.535593 (2023), doi: <https://doi.org/10.1101/2023.04.17.535593>.
- [17] Y.-H. Tseng, Onset of movement in a one-dimensional active gel model of cell motility, MS thesis, National Central University, 2020, http://140.113.39.130/cgi-bin/g32/ncugsweb.cgi/ccd=EQD_qa/webmgswitchlang=en.
- [18] It is known that an adhesion complex under an external force exhibits treadmilling in the direction of force [12]. This treadmilling is due to the dissociation of proteins on one side and the association of proteins on the other side of the adhesion complex, and the treadmilling speed is small compared to the cytoplasmic flow. Our model does not include this effect.
- [19] R. Meili and R. A. Firtel, Two poles and a compass, *Cell* **114**, 153 (2003).
- [20] Y. T. Maeda, J. Inose, M. Y. Matsuo, S. Iwaya, and M. Sano, Ordered patterns of cell shape and orientational correlation during spontaneous cell migration, *PLoS ONE* **3**, e3734 (2008).
- [21] F. Wang, P. Herzmark, O. D. Weiner, S. Srinivasan, G. Servant, and H. R. Bourne, Lipid products of PI(3)Ks maintain persistent cell polarity and directed motility in neutrophils, *Nat. Cell Biol.* **4**, 513 (2002).
- [22] J. Xu, F. Wang, A. Van Keymeulen, P. Herzmark, A. Straight, K. Kelly, Y. Takuwa, N. Sugimoto, T. Michison, and H. R. Bourne, Divergent signals and cytoskeletal assemblies regulate self-organizing polarity in neutrophils, *Cell* **114**, 201 (2003).
- [23] T. Y.-C. Tsai, S. R. Collins, C. K. Chan, A. Hadjitheorou, P.-Y. Lam, S. S. Lou, H. W. Yang, J. Jorgensen, F. Ellett, D. Irimia, M. W. Davidson, R. S. Fischer, A. Huttenlocher, T. Meyer, J. E. Ferrell Jr., and J. A. Theriot, Efficient front-rear coupling in neutrophil chemotaxis by dynamic myosin II localization, *Dev. Cell* **49**, 189 (2019).
- [24] C. S. Peskin, G. M. Odell, and G. F. Oster, Cellular motions and thermal fluctuations: The Brownian ratchet, *Biophys. J.* **65**, 316 (1993).
- [25] P. Recho, T. Putelat, and L. Truskinovsky, Active gel segment behaving as an active particle, *Phys. Rev. E* **100**, 062403 (2019).
- [26] T. P. Lele, J. Pendse, S. Kumar, M. Salanga, J. Karavitis, and D. E. Ingber, Mechanical forces alter zyxin unbinding kinetics within focal adhesions of living cells, *J. Cell Physiol.* **207**, 187 (2006).
- [27] K. Dierkes, A. Sumi, J. Solon, and G. Salbreux, Spontaneous oscillations of elastic contractile materials with turnover, *Phys. Rev. Lett.* **113**, 148102 (2014).
- [28] J.-Y. Lo and H.-Y. Chen (unpublished).
- [29] H. Tanimoto and M. Sano, A simple force-motion relation for migrating cells revealed by multipole analysis of traction stress, *Biophys. J.* **106**, 16 (2014).
- [30] T. Ohta, M. Tarama, and M. Sano, Simple model of cell crawling, *Physica D* **318-319**, 3 (2016).
- [31] T. Luo, K. Mohan, V. Srivastava, Y. Ren, P. A. Iglesias, and D. N. Robinson, Understanding the cooperative interaction between myosin II and actin cross-linkers mediated by actin filaments during mechanosensation, *Biophys. J.* **102**, 238 (2012).
- [32] P. Monzo, M. Crestani, Y. K. Chong, A. Ghisleni, K. Hennig, Q. Li, N. Kakogiannos, M. Giannotta, C. Richichi, T. Dini, E. Dejana, P. Maiuri, M. Balland, M. P. Sheetz, G. Pelicci, B. T. Ang, C. Tang, and N. C. Gauthier, Adaptive mechanoproperties mediated by the formin FMN1 characterize glioblastoma fitness for invasion, *Develop. Cell* **56**, 2841 (2021).
- [33] E. L. Barnhart, K.-C. Lee, K. Keren, A. Mogilner, and J. A. Theriot, An adhesion-dependent switch between mechanisms that determine motile cell shape, *PLoS Biol.* **9**, e1001059 (2011).
- [34] R. Milo and R. Phillips, *Cell Biology by the Numbers* (Garland Science, 2015).
- [35] E. Urban, S. Jacob, M. Nemethova, G. P. Resch, and J. V. Small, Electron tomography reveals unbranched networks of actin filaments in lamellipodia, *Nat. Cell Biol.* **12**, 429 (2010).
- [36] Y.-L. Wang, Reorganization of actin filament bundles in living fibroblasts, *J. Cell Biol.* **99**, 1478 (1984).
- [37] D. Shao, H. Levine, and W.-J. Rappel, Coupling actin flow, adhesion, and morphology in a computational cell motility model, *Proc. Natl. Acad. Sci. USA* **109**, 6851 (2012).